NANO LETTERS

Letter

pubs.acs.org/NanoLett

Influence of Droplet Size on the Growth of Self-Catalyzed Ternary GaAsP Nanowires

Yunyan Zhang,*[,†] Ana M. Sanchez,[‡] Yue Sun,[#] Jiang Wu,[†] Martin Aagesen,[§] Suguo Huo,[∥] Dongyoung Kim,[†] Pamela Jurczak,[†] Xiulai Xu,[#] and Huiyun Liu[†]

[†]Department of Electronic and Electrical Engineering, University College London, London WC1E 7JE, United Kingdom

[‡]Department of Physics, University of Warwick, Coventry CV4 7AL, United Kingdom

[#]Beijing National Laboratory for Condensed Matter Physics, Institute of Physics, Chinese Academy of Sciences, Beijing 100190, People's Republic of China

[§]Gasp Solar ApS, Gregersensvej 7, Taastrup DK−2630, Denmark

[∥]London Centre for Nanotechnology, University College London, London WC1H 0AH, United Kingdom

ABSTRACT: The influences of droplet size on the growth of self-catalyzed ternary nanowires (NWs) were studied using GaAsP NWs. The size-induced Gibbs−Thomson (GT) effect makes the smaller catalytic droplets have lower effective supersaturations and hence slower nucleation rates than the larger ones. Large variation in droplet size thus led to the growth of NWs with low uniformity, while a good size uniformity of droplets resulted in the production of highly uniform NWs. Moreover, thinner NWs were observed to be richer in P, indicating that P is more resistant to the GT effect than As because of a higher chemical potential inside Ga droplets. These results provide useful information for understanding the mechanisms of self-catalyzed III−V NW nucleation and growth with the important ternary III−V material systems.

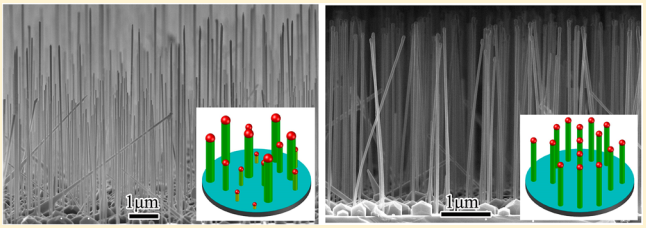

KEYWORDS: *Nanowire, droplet size, self−catalyzed, Gibbs−Thomson effect, GaAsP, uniformity, chemical potential*

The research on III−V nanowires (NWs) has intensified over the last two decades due to their potential use in electronic and optoelectronic devices.[1−3] Their one-dimensional geometry at nanometer scale can lead to different crystallographic,[4,5] photonic,[6−8] electrical,[9,10] and mechanical[11] properties than those of their thin film counterparts. These novel properties can be employed to develop devices with superior performance in a broad range of applications including diodes, sensors, and photocatalysis.[12−15]

Droplet-catalyzed growth is one of the most popular techniques for fabrication of NWs. In this mode, catalytic droplets are needed to achieve the vapor−liquid−solid (VLS) growth,[16] which is significantly different from the traditional thin film growth using the vapor−solid mode. Despite great efforts, the detailed nucleation mechanisms of this growth mode are still unclear, particular due to the size of the catalytic droplet being in nanometre scale. The influences caused by the small droplet size can greatly affect the NW growth and hence modify the performances of the reactants.[17] For example, the Gibbs−Thomson (GT) effect can increase the vapor pressure of droplets and hence decrease the effective supersaturation inside.[18,19] It is well-established that the droplet supersaturation is a crucial factor for the NW growth, impacting NW growth direction, growth rate, and crystal structure.[20−23] Although there are some studies of the droplet size effect on Au-catalyzed NW growth,[24−27] to our knowledge there is no report on self-catalyzed NW growth. Since Au-catalyzed NWs are considered incompatible with complementary metal−oxide−semiconductor (CMOS) industrial standards, it is thus critical to study the impact of the droplet's size on self−catalyzed NWs to further improve the performance of III−V on Si NW devices.

Currently, most of the studies on self-catalyzed NW growth are focused on binary material systems. In order to obtain more freedom in adjusting the energy band gap, ternary material systems are needed.[28−30] For self-catalyzed growth, ternary III−V NWs prefer the material combinations of one group−III element and two group−V elements, such as GaAsP.[31−33] During the growth, they are under group−III element rich condition and the group−V elements govern the supersaturation of the droplets.[34] Due to the high vapor pressure of the group−V elements their incorporation into NWs is very sensitive to the growth environment and can hence be significantly modified by the droplet's size due to for instance the GT effect. In addition, different group-V elements have different chemical potentials, making the influences of the droplet's size different on each of them.[35−37] Thus, the nucleation and growth of a particular material composition in ternary NWs is complicated.

Received: November 8, 2015
Revised: December 13, 2015
Published: December 26, 2015

DOI: 10.1021/acs.nanolett.5b04554
Nano Lett. 2016, 16, 1237−1243

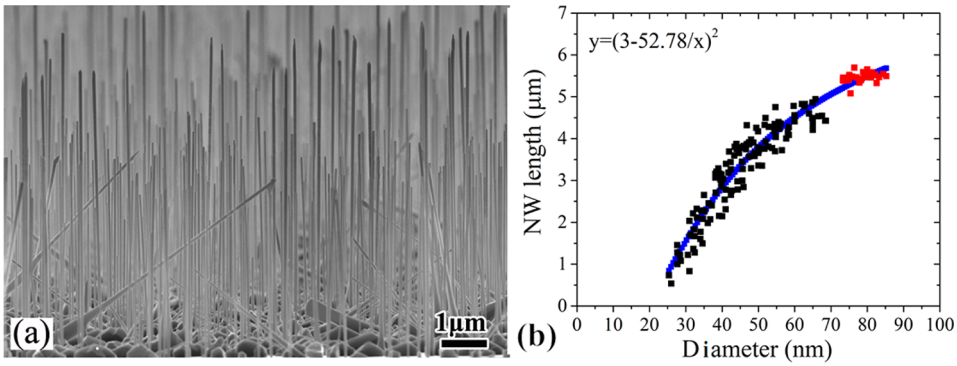

Figure 1. (a) Side-view SEM image and (b) length-diameter summation of GS-GaAsP NWs grown at ~635 °C. The blue line in b is the fitting curve described by the inset equation. The red dots in b are corrected by reducing the actual length by 5/60, because their growth time was 5 min longer compared with black dots which can be referred to Figure 4 for further information.

When using the NWs for the device fabrication after growth, a good NW uniformity is favorable, because it can greatly facilitate the fabrication process and hence reduce the cost. On the other hand, highly nonuniform NWs have some advanced properties that can greatly improve the device performance. For example, resonant optical modes inside NWs are strongly diameter-, length-, and period-dependent.[38−40] If the devices are made of NWs with random position, diameter, and/or length, broad band optical enhancement is expected as compared with uniform arrays.[41,42] This is highly favorable for fabricating high-efficiency photovoltaics and photodetections. Therefore, depending on different objectives, the NW needs to be controlled to be highly uniform or nonuniform. However, most of the uniformity control is achieved by using patterned substrates or Au-catalyzed mode that are either expensive or limited by the potential Au contamination. The development of uniformity control technique for self-catalyzed NWs on nonpatterned substrates can provide a way to produce high-performance but low-cost NW devices.

Here we present, for the first time, observations of the GT effect in the self-catalyzed growth mode using GaAsP NWs. Due to this effect, NWs grown from smaller droplets exhibit slower growth rates and have higher P contents compared with those produced from larger ones. By controlling droplet size uniformity, growths of highly uniform and highly nonuniform NWs have been demonstrated. The crystallographic and optical properties of NWs with different uniformities were also studied.

The self-catalyzed GaAsP and GaAs nanowires were grown directly on p-type Si(111) substrates by means of solid-source III−V MBE. There were two approaches used for the GaAsP NW growth. In the first approach, growth was initiated with a GaAs stem for 5 min and then followed by a 55 min GaAsP growth, which are called GaAs-stem GaAsP NWs (GS-GaAsP NWs) for simplicity. The other growth method started directly with GaAsP and lasted for 1 h, which is called directly grown GaAsP NWs (DG-GaAsP NWs). If not indicated otherwise, the GaAs stem was grown with a Ga beam equivalent pressure of 1.12×10^{-7} Torr and V/III flux ratio of 60 at ~640 °C. The GaAsP segments of both types of NWs were grown with a Ga beam equivalent pressure, V/III flux ratio, P/(As+P) flux ratio, and substrate temperature of 1.12×10^{-7} Torr, 50, 0.12, and ~640 °C, respectively. GaAs NWs were grown with a Ga beam equivalent pressure, V/III flux ratio, substrate temperature, and growth duration of 1.12×10^{-7} Torr, 44, ~630 °C, and 1 h, respectively. The substrate temperature was measured by a pyrometer. The NW morphology was measured with a Zeiss XB 1540 focus ion beam/scanning electron microscope (FIB/SEM) system. Simple scraping of the NWs onto a lacey carbon support was used to prepare transmission electron microscopy (TEM) specimens. The TEM measurements were performed on JEOL 2100 and doubly-corrected ARM200F microscopes, both operating at 200 kV. Compositional analysis using energy-dispersive X-ray spectrometry (EDX) was performed using Oxford Instruments 100 mm^2 SDD EDX detectors. Power-dependent photoluminescence (PL) spectroscopy was measured by a confocal microphotoluminescence system with a laser spot diameter of ~2 μm, and the spectra were detected with a liquid nitrogen cooled charge coupled device camera. Room-temperature PL measurement was performed using a nanometrics RPM2000 machine with excitation wavelength of 635 nm and power density of ~500 W/cm^2.

The morphology of GS-GaAsP NWs grown at ~635 °C is shown in Figure 1a. It can be observed that the lengths of GaAsP NWs vary significantly. This large length variation is connected with the NW diameter differences. As can be seen from the diameter-length summation in Figure 1b, the NWs with larger diameters are generally longer. This can be explained by the GT effect, which can significantly increase the balanced vapor pressure of the droplets, especially the vapor pressure of group V elements.[18,19] For the smaller droplets, the vapor pressure can be increased more than that of the larger ones. Therefore, the effective supersaturation $\Delta\mu$ (the effective difference between the chemical potentials of elements in the vapor phase and in the NW) inside the droplet with a smaller diameter is lower, which can be expressed as[19,43]

$$\Delta\mu = \Delta\mu_0 - 4\Omega\alpha_{vs}/d \quad (1)$$

where the $\Delta\mu_0$ is the supersaturation in the planar limit (i.e., $d \rightarrow \infty$), Ω is the atomic volume of the growth species, d is the diameter of the NW, and α_{vs} is the average surface energy density of the NW surface facets. The growth rate strongly depends on the supersaturation and can be expressed as[19,43]

$$v = \left(\frac{\sqrt{b}\,\Delta\mu}{kT}\right)^2 = \left(\frac{\sqrt{b}\,\Delta\mu_0}{kT} - \frac{\sqrt{b}\,4\Omega\alpha_{vs}}{kTd}\right)^2 \quad (2)$$

where b is a kinetic coefficient of crystallization, k is Boltzmann's constant, and T is the temperature. Thus, the reduction of the $\Delta\mu$ can slow down the growth rate. With the growth time of t, the NW length can be expressed as[19,43]

DOI: 10.1021/acs.nanolett.5b04554
Nano Lett. 2016, 16, 1237−1243

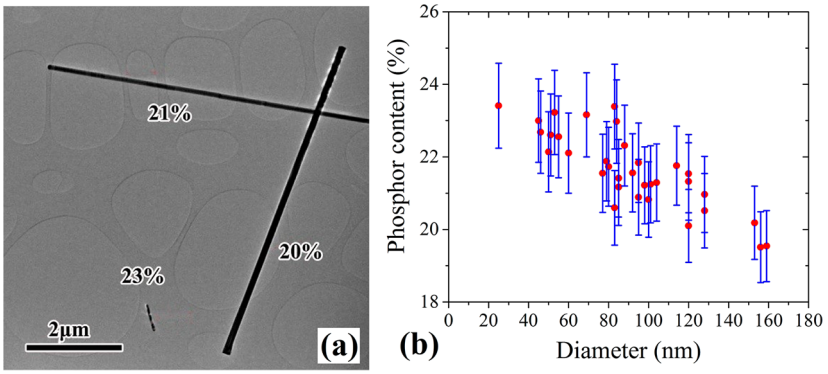

Figure 2. (a) Phosphorus content of GS-GaAsP NWs with different diameters. (b) Phosphorus content VS NW diameter.

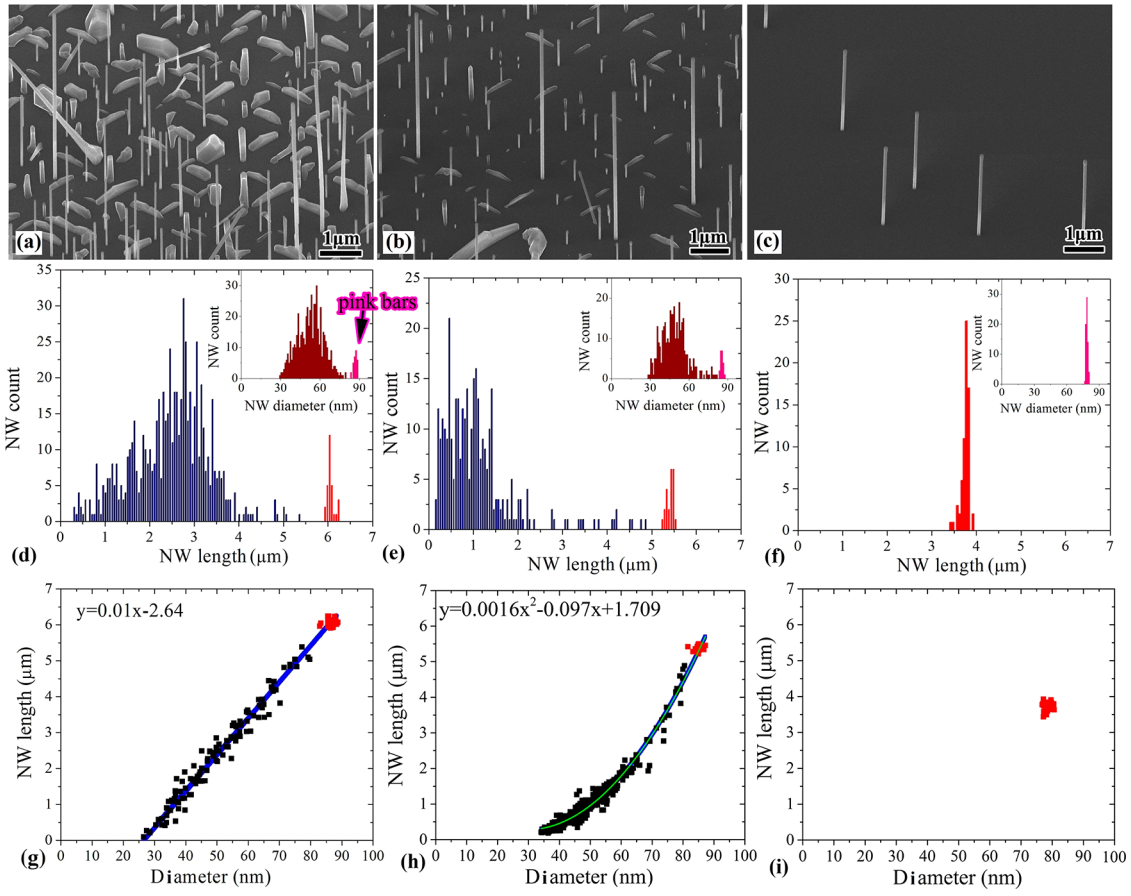

Figure 3. 35° tilted SEM image, length summation histogram, and diameter-length relationship of GS-GaAsP NWs grown at (a, d, g) ~640 °C, (b, e, h) ~645 °C, and (c, f, i) ~650 °C. The insets in d, e, and f are the diameter summation histograms. The red columns in d–f and dots in g–h are corrected by reducing the actual length by 5/60, which is the same as Figure 1b. The blue lines in g and h are the fitting curves described by the inset equations. The green line in h is the same as the blue line which was added to improve the clarity of the plot.

$$L = vt = \left(\frac{\sqrt{b}\,\Delta\mu_0 t^2}{kT} - \frac{\sqrt{b}\,4\Omega\alpha_{vs} t^2}{kTd} \right)^2 \quad (3)$$

By defining $A = (b^{1/2}\Delta\mu_0 t^2/kT)$ and $B = (b^{1/2}4\Omega\alpha_{vs}t^2/kTd)$, L can be expressed as

$$L = \left(A - \frac{B}{d} \right)^2 \quad (4)$$

eq 4 fits the experiment data well with $A = 3$ and $B = 52.78$.

Another explanation for the variation in length could be that there is constant nucleation of new Ga-catalyzed nanowires throughout the growth, but with less Ga available to form the droplet as a function of time. This explanation does however not fit the results obtained in the comparative growths described later in the text.

To further examine the influence of the GT effect on the NW growth, the P content of GS-GaAsP NWs with different diameters was studied. As shown in Figure 2, the NW with a smaller diameter is higher in P content, which is consistent with the GT effect. During the growth, the droplet vapor pressure can be significantly increased as the size decreases due to the GT effect.[18,19,43] This results in the smaller droplets having a stronger driving force to push out the group V elements inside

DOI: 10.1021/acs.nanolett.5b04554
Nano Lett. 2016, 16, 1237–1243

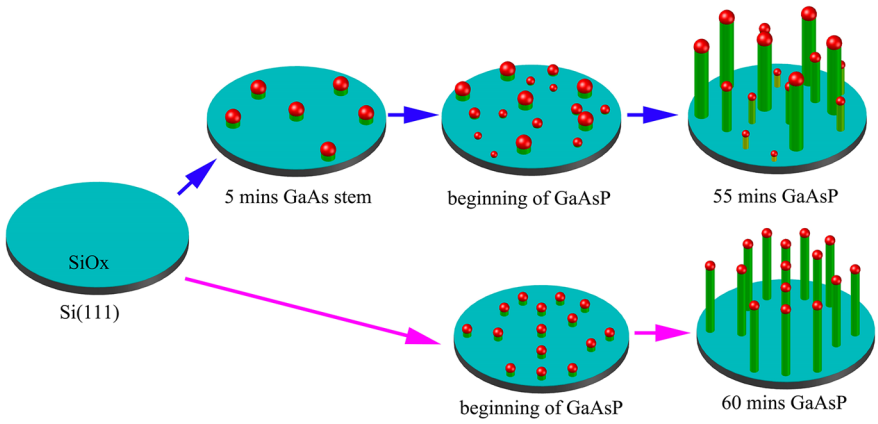

Figure 4. Growth mechanism illustration of GaAsP NWs grown with (GS NWs) and without (DG NWs) GaAs stems.

to lower the effective supersaturation, as well as a higher barrier for incorporating new group V atoms. Thus, the incorporation efficiencies of group V elements in droplets with a smaller size were reduced as compared with those of larger ones. The higher P content in smaller NW suggests P here has a higher incorporation probability than As during growth. This occurs because P has a higher chemical potential with Ga in comparison to As, and hence stronger nucleation ability.[37] As a result, its reduction in the incorporation efficiency was smaller when the droplet size decreased, making the smaller NW richer in P.

The influence of the growth temperature on NWs of different diameters was also studied. At the growth temperature of ~640 °C, the NWs can be roughly divided into two groups by their diameters, forming a bimodal distribution. The NWs in the large-diameter group are much longer (~6 μm) and uniform in both length and diameter, which can be seen from the red columns in Figure 3d and the pink columns in the inset. In contrast, the NWs from the small-diameter group are much shorter (peak length ~2.5 μm) and have a much wider distribution in both length and diameter, which can be seen from the blue columns in Figure 3d and the brown columns in the inset. With the increase of the growth temperature to ~645 °C, the size distribution of NWs did not change significantly, as can be seen in the inset of Figure 3e. However, their length decreased rapidly, which is shown in Figure 3e. Compared to the NWs in the large-diameter group, the length reduction rate ($\Delta L/L_0$), where ΔL is the length reduction and L_0 is the length of NWs, Figure 3a sample) of the ones in the small-diameter group is much larger. Further increase of the growth temperature to ~650 °C caused complete suppression of the growth of small-diameter NWs, leaving only large-diameter NWs with small density but good length and diameter uniformity, as shown in Figure 3f. These phenomena can be due to the temperature-dependent change in droplet supersaturation. With the increase of the growth temperature, droplet supersaturation decreases, which can slow down the nucleation and hence reduce growth rate.[37,44] When the temperature is higher than the critical value, the supersaturation of the droplets can be too low to maintain the NW growth. For smaller droplets, their critical temperature is lower because the GT effect can give them extra reduction in supersaturation as compared with larger ones, making the small-diameter NW group disappear at ~650 °C.[43,45]

For each growth temperature, as shown in Figure 3g and h, NWs with larger diameters are in general longer, which is similar to Figure 1b. However, the relationship between the diameter and length is changed to almost linear in Figure 3g and then to parabolic in Figure 3h. These phenomena clearly show that the nucleation and growth rate differences between the large and small NWs were enlarged with the increase of the growth temperature. This could however be due to the material desorption from the wafer surface. During the growth, some III−V materials deposited on the wafer surface can desorb back to vapor phase. Part of these desorbed materials, Ga, As, and P, can still contribute to the NW growth, because they can impinge on the NW sidewalls and then diffuse to the droplets, which is called secondary absorption. Therefore, the longer NWs have an advantage in collecting the desorbed materials, which can enhance their growth rate. With the increase of the growth temperature, the III−V materials desorption from the wafer surface can be greatly enhanced. The amount of materials deposited on the wafer surface has been reduced significantly at higher temperatures, which can be seen in Figure 3a−c. This can boost sidewall material collection and hence the growth rate difference between long (thick) and short (thin) NWs.

According to the above observations, the model proposed in Figure 4 could explain the large variation in NW length and diameter during the growth of GS-GaAsP NWs. At the beginning of the GaAs stem growth, there was no material deposition on the substrate surface, which is beneficial for the formation of droplets with uniform diameters. Because growth temperature was 5−10 °C higher than conventional GaAs NW growth, the droplets for the GaAs stem growth were quite large and hence led to NWs with large diameters (~90 nm). These NWs correspond to the large-diameter NW group shown in Figure 3. Introduction of the P flux for GaAsP growth can significantly increase the chemical potential of the vapor phase.[46] This can promote the formation of the second batch of droplets. Due to the strong competition and interference from the first-batch GaAs stems, the inferior Ga collection environment made the size of the second−batch droplets much smaller and nonuniform. During the subsequent NW growth, the strong GT effect gave the smaller droplets higher vapor pressures. As a result, the effective supersaturation inside was lower, making them slower in nucleation rate and hence shorter. The droplet size distribution could thus govern the NW uniformity. Consequently, it is important to keep a constant chemical potential of the vapor phase for the formation of uniform droplet size to achieve uniform NW growth. To prove this, GaAsP NWs were grown without the GaAs stem and in addition, pure GaAs NWs were grown as a

DOI: 10.1021/acs.nanolett.5b04554
Nano Lett. 2016, 16, 1237−1243

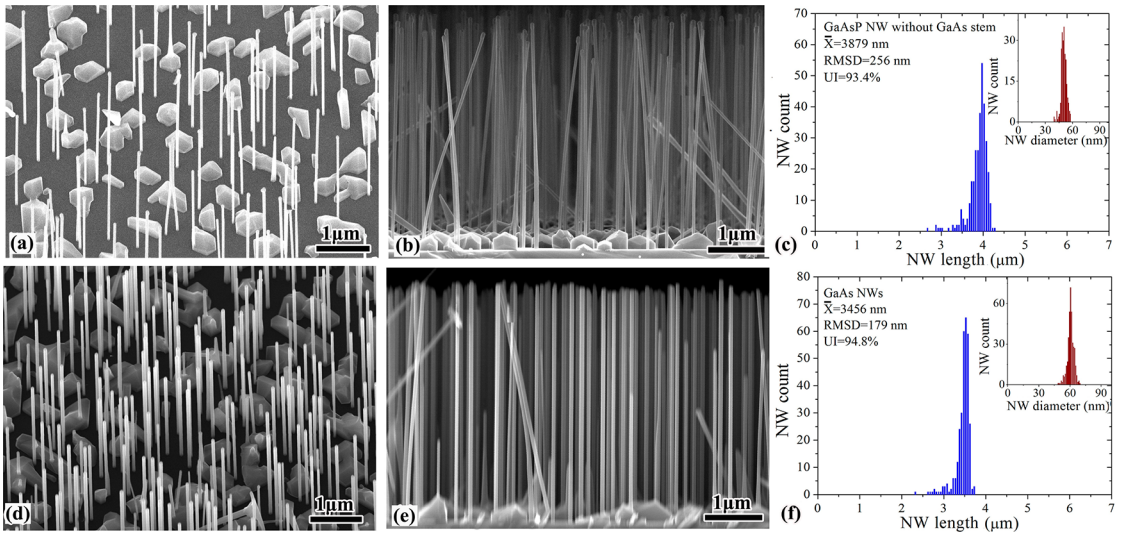

Figure 5. (a) 35° tilted view SEM image, (b) side view SEM image, and (c) length summation histogram of DG-GaAsP NWs. (d) 25° tilted view SEM image, (e) side view SEM image, and (f) length summation histogram of GaAs NWs. The inset in c and f are the diameter summation histograms of each sample.

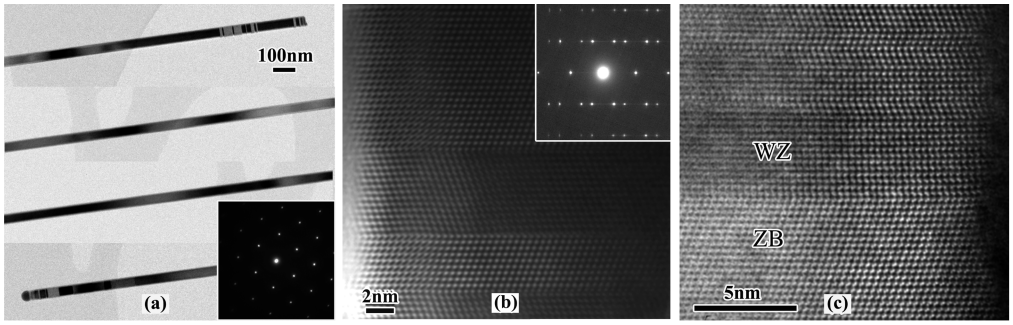

Figure 6. (a) TEM images of a GaAsP NW. The inset is an electron diffraction pattern taken from the middle part of the NW. (b) Atomic level resolution TEM image of the bottom part of the NW. The inset is an electron diffraction pattern. (c) Atomic level resolution TEM image of the NW tip.

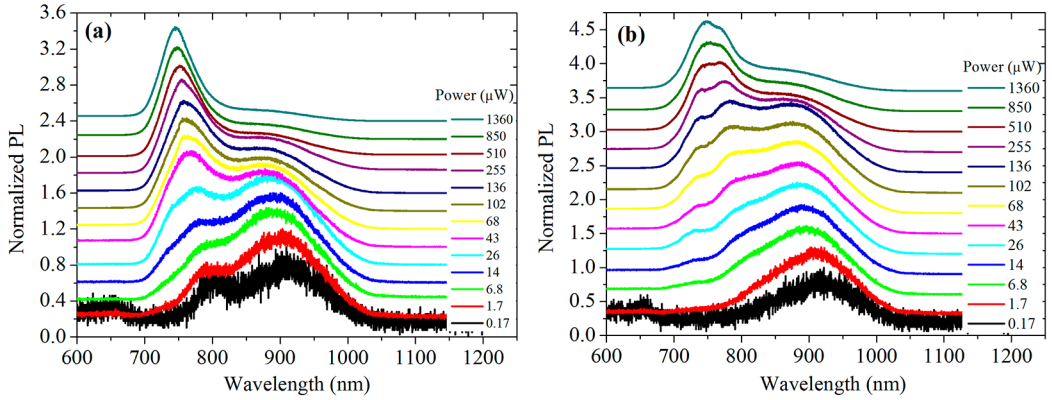

Figure 7. 10 K power-dependent PL measurement of (a) DG-GaAsP NWs and (b) GS-GaAsP NWs.

reference. There was no change in growth parameters during the growths to provide a comparatively stable environment. The results are shown in Figure 5. Both GaAsP and GaAs NWs are highly uniform in length and diameter. The average NW length ($\bar{X}$), root-mean-square deviation (RMSD) and uniformity index (UI) are used to describe the NW length information and are defined by the following equations:

$$\bar{X} = \frac{1}{n}\sum_{i=1}^{n} X_i \tag{5}$$

$$\mathrm{RMSD} = \sqrt{\frac{1}{n}\sum_{i=1}^{n}(X_i - \bar{X})^2} \tag{6}$$

$$\mathrm{UI} = 100\%*(\bar{X} - \mathrm{RMSD})/\bar{X} \tag{7}$$

DOI: 10.1021/acs.nanolett.5b04554
Nano Lett. 2016, 16, 1237−1243

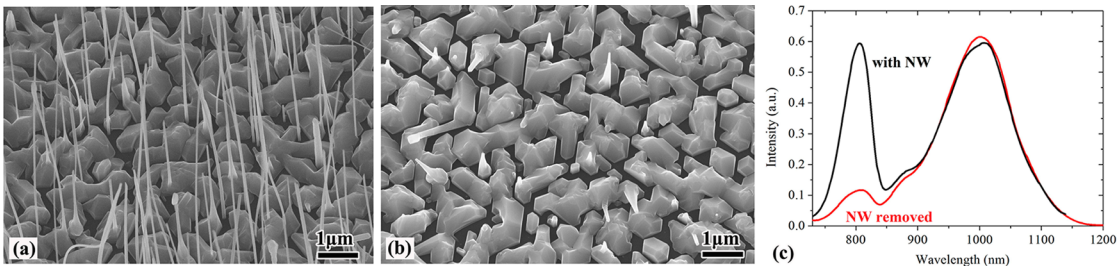

Figure 8. SEM images of GaAsP NW sample (a) before and (b) after the NW removal by ultrasonic bath. (c) Room-temperature PL measurement of the samples from a and b.

where the n is the number of NWs that were used in the summation.

The $\bar{X}$ of GaAsP and GaAs NWs are 3879 and 3456 nm, respectively. The RMSD is only 256 nm for GaAsP and 179 nm for GaAs NWs. Therefore, the UI is as high as 93.4% for GaAsP and 94.8% for GaAs NWs. This is in stark contrast with the GS-GaAsP NWs shown in Figure 3a that has an $\bar{X}$, RMSD, and UI of 2557 nm, 888 nm, and 65.3%, respectively.

The crystal quality of those NWs was checked by TEM measurements. All of the GaAsP NWs have quite similar features. One representative NW is shown in Figure 6a. Zinc blend (ZB) crystal structure dominates this NW. The body part is pure ZB and free of any defects. Defects are present at the very tip and very bottom parts. Most of the defects at the bottom part of the NW are single twins, which can be seen in Figure 6b. This could be due to the slight fluctuation of growth environment at the initial stage. On the other hand, at the tip of the NW, along with the single twins, there are wurtzite segments. As can be seen in Figure 6c, the segments can be as long as several nanometers on some occasions. These defects at the tip should be due to the change of growth parameters during the termination of the NW growth.

The optical properties of the GS- and DG-GaAsP NWs were characterized by PL measurements. Two major peaks were observed in both samples as can be seen in Figure 7. The first peak is around 750 nm at 10 K. The intensity of this peak is much stronger at high excitation powers but decreases much faster with reduction of excitation power compared with the other peak. The emissions from the NWs should be the major contribution to this peak. The high surface-to-volume ratio results in NWs having a high density of surface states. Therefore, at low excitation power, most of the generated carriers were consumed rapidly at the surface states through nonradiative recombinations. This resulted in low emission intensity. However, the NWs have very good crystal quality with low defect density. Most importantly, they have no threading dislocations that can contribute to the nonradiative recombinations. Therefore, as the surface states were getting saturated with the increase of excitation power, the emission efficiency and hence PL intensity increased rapidly. It needs to be mentioned that the peak from the GS−GaAsP NWs is much broader compared with that of the NWs without GaAs stems. This could be because GS-GaAsP NWs have a large variation in size and composition. Moreover, the spectra from GS−GaAsP NWs are actually merged from two small peaks. This could be explained by their bimodal NW distribution shown in Figure 3. The second peak is around 920 nm at low temperature. It is weaker but comparatively less sensitive to excitation power than the 750 nm peak. In order to identify the origin of this peak, GS-GaAsP NWs were grown at ∼630 °C to produce NWs as well as high-density parasitic clusters. Room-temperature PL measurement was performed on the sample before (Figure 8a) and after (Figure 8b) NW removal. As can be seen in Figure 8c, at room temperature, this peak is centered at around 1000 nm. Before and after the NW removal, the intensity of this peak did not change significantly. In contrast, the NW peak decreased dramatically. Therefore, the parasitic grown clusters should be the main origin of the emission at 1000 nm (room temp. measurement). It could be due to the defects caused by group-III rich growth environment, such as Ga antisite defects and/or group-V Schottky defects.[47−49]

In conclusion, the influences of the droplet size on growth of self-catalyzed ternary NWs were studied using GaAsP NWs. Nanoscale dimension of the catalytic droplets cause them to be influenced by the GT effect. With the decrease of the droplet size, the influence from the GT effect is stronger, resulting in smaller droplets having lower supersaturation and hence a slower nucleation rate. By controlling the size uniformity of the catalyst droplets, through varying the chemical potential of the vapor phase, the growth of both highly uniform and highly nonuniform NW heights have been demonstrated. Furthermore, the droplet size was observed to also influence the NW composition, with thinner GaAsP NWs found to be richer in P. This could be explained by the fact that P has higher chemical potential with Ga and hence stronger nucleation ability, which make it more resistant to the GT effect than As. These results not only give valuable information for understanding the NW nucleation mechanisms, but also provide additional knowledge on how to control composition and uniformity of the NWs.

AUTHOR INFORMATION

Corresponding Author

*E-mail: yunyan.zhang.11@ucl.ac.uk.

Notes

The authors declare no competing financial interest.

ACKNOWLEDGMENTS

The authors acknowledge the support of Leverhulme Trust. H. Liu would like to thank The Royal Society for funding his University Research Fellowship. X. Xu would like to thank the financial support from NSFC (91436101, 11174356, and 61275060) and Chinese Academy of Sciences (XDB07030200).

REFERENCES

(1) Lieber, C. M.; Wang, Z. L. *MRS Bull.* **2007**, *32*, 99−108.
(2) Yan, R.; Gargas, D.; Yang, P. *Nat. Photonics* **2009**, *3*, 569−576.
(3) Yang, P.; Yan, R.; Fardy, M. *Nano Lett.* **2010**, *10*, 1529−1536.
(4) Caroff, P.; Dick, K. A.; Johansson, J.; Messing, M. E.; Deppert, K.; Samuelson, L. *Nat. Nanotechnol.* **2009**, *4*, 50−55.

DOI: 10.1021/acs.nanolett.5b04554
Nano Lett. 2016, 16, 1237−1243

(5) Assali, S.; Zardo, I.; Plissard, S.; Kriegner, D.; Verheijen, M. A.; Bauer, G.; Meijerink, A.; Belabbes, A.; Bechstedt; Haverkort, J. E. M.; Bakkers, E. P. A. M. *Nano Lett.* **2013**, *13*, 1559−1563.
(6) Wilhelm, C.; Larrue, A.; Dai, X.; Migas, D.; Soci, C. *Nanoscale* **2012**, *4*, 1446−1454.
(7) Scofield, A. C.; Kim, S.−H.; Shapiro, J. N.; Lin, A.; Liang, B.; Scherer, A.; Huffaker, D. L. *Nano Lett.* **2011**, *11*, 5387−5390.
(8) Lopez, F. J.; Hemesath, E. R.; Lauhon, L. J. *Nano Lett.* **2009**, *9*, 2774−2779.
(9) Parkinson, P.; Joyce, H. J.; Gao, Q.; Tan, H. H.; Zhang, X.; Zou, J.; Jagadish, C.; Herz, L. M.; Johnston, M. B. *Nano Lett.* **2009**, *9*, 3349−3353.
(10) Wallentin, J.; Ek, M.; Wallenberg, L. R.; Samuelson, L.; Borgström, M. T. *Nano Lett.* **2012**, *12*, 151−155.
(11) Bao, P.; Wang, Y.; Cui, X.; Gao, Q.; Yen, H.; Liu, H.; Yeoh, W. K.; Liao, X.; Du, S.; Tan, H. H.; Jagadish, C.; Zou, J.; Ringer, S. P.; Zheng, R. *Appl. Phys. Lett.* **2014**, *104*, 021904.
(12) LaPierre, R. R. *J. Appl. Phys.* **2011**, *110*, 014310.
(13) Zhang, Y.; Wu, J.; Aagesen, M.; Liu, H. *J. Phys. D: Appl. Phys.* **2015**, *48*, 463001.
(14) Nguyen, H. P. T.; Zhang, S.; Connie, A. T.; Kibria, M. G.; Wang, Q.; Shih, I.; Mi, Z. *Nano Lett.* **2013**, *13*, 5437−5442.
(15) Krogstrup, P.; Jørgensen, H. I.; Heiss, M.; Demichel, O.; Holm, J. V.; Aagesen, M.; Nygard, J.; Fontcuberta i Morral, A. F. *Nat. Photonics* **2013**, *7*, 306−310.
(16) Wagner, R. S.; Ellis, W. C. *Appl. Phys. Lett.* **1964**, *4*, 89−90.
(17) Johansson, J.; Dick, K. A.; Caroff, P.; Messing, M. E.; Bolinsson, J.; Deppert, K.; Samuelson, L. *J. Phys. Chem. C* **2010**, *114*, 3837−3842.
(18) Ek, M.; Borg, B. M.; Johansson, J.; Dick, K. A. *ACS Nano* **2013**, *7*, 3668−3675.
(19) Givargizov, E. I. *J. Cryst. Growth* **1975**, *31*, 20−30.
(20) Johansson, J.; Karlsson, L. S.; Dick, K. A.; Bolinsson, J.; Wacaser, B. A.; Deppert, K.; Samuelson, L. *Cryst. Growth Des.* **2009**, *9*, 766−773.
(21) Russo-Averchi, E.; Heiss, M.; Michelet, L.; Krogstrup, P.; Nygard, J.; Magen, C.; Morante, J. R.; Uccelli, E.; Arbiol, J.; Fontcuberta i Morral, A. *Nanoscale* **2012**, *4*, 1486−1490.
(22) Krogstrup, P.; Popovitz-Biro, R.; Johnson, E.; Madsen, M. H.; Nygård, J.; Shtrikman, H. *Nano Lett.* **2010**, *10*, 4475−4482.
(23) Rudolph, D.; Hertenberger, S.; Bolte, S.; Paosangthong, W.; Spirkoska, D.; Döblinger, M.; Bichler, M.; Finley, J. J.; Abstreiter, G.; Koblmüller, G. *Nano Lett.* **2011**, *11*, 3848−3854.
(24) Fröberg, L. E.; Seifert, W.; Johansson, J. *Phys. Rev. B: Condens. Matter Mater. Phys.* **2007**, *76*, 153401.
(25) Lugani, L.; Ercolani, D.; Beltram, F.; Sorba, L. *J. Cryst. Growth* **2011**, *323*, 304−306.
(26) Kashchiev, D. *Cryst. Growth Des.* **2006**, *6*, 1154−1156.
(27) Dubrovskii, V. G.; Sibirev, N. V.; Cirlin, G. E.; Soshnikov, I. P.; Chen, W. H.; Larde, R.; Cadel, E.; Pareige, P.; Xu, T.; Grandidier, B.; Nys, J.−P.; Stievenard, D.; Moewe, M.; Chuang, L. C.; Chang-Hasnain, C. *Phys. Rev. B: Condens. Matter Mater. Phys.* **2009**, *79*, 205316.
(28) Holm, J. V.; Jørgensen, H. I.; Krogstrup, P.; Nygård, J.; Liu, H.; Aagesen, M. *Nat. Commun.* **2013**, *4*, 1498.
(29) Zhang, Y.; Sanchez, A. M.; Wu, J.; Aagesen, M.; Holm, J. V.; Beanland, R.; Ward, T.; Liu, H. *Nano Lett.* **2015**, *15*, 3128−3133.
(30) Zhang, Y.; Wu, J.; Aagesen, M.; Holm, J.; Hatch, S.; Tang, M.; Huo, S.; Liu, H. *Nano Lett.* **2014**, *14*, 4542−4547.
(31) Paek, J.; Yamaguchi, M.; Amano, H. *J. Cryst. Growth* **2011**, *323*, 315−318.
(32) Wu, J.; Li, Y.; Kubota, J.; Domen, K.; Aagesen, M.; Ward, T.; Sanchez, A.; Beanland, R.; Zhang, Y.; Tang, M.; Hatch, S.; Seeds, A.; Liu, H. *Nano Lett.* **2014**, *14*, 2013−2018.
(33) Heiss, M.; Ketterer, B.; Uccelli, E.; Morante, J. R.; Arbiol, J.; Fontcuberta i Morral, A. *Nanotechnology* **2011**, *22*, 195601.
(34) Dubrovskii, V. G. *Appl. Phys. Lett.* **2014**, *104*, 053110.
(35) Lany, S. *Phys. Rev. B: Condens. Matter Mater. Phys.* **2008**, *78*, 245207.
(36) Ansara, I.; Chatillon, C.; Lukas, H. L.; Nishizawa, T.; Ohtani, H.; Ishida, K.; Hillert, M.; Sundman, B.; Hillert, M.; Sundman, B.; Argent, B. B.; Watson, A.; Chart, T. G.; Anderson, T. *CALPHAD: Comput. Coupling Phase Diagrams Thermochem.* **1994**, *18*, 177−222.
(37) Glas, F. *J. Appl. Phys.* **2010**, *108*, 073506.
(38) Wu, P. M.; Anttu, N.; Xu, H. Q.; Samuelson, L.; Pistol, M. E. *Nano Lett.* **2012**, *12*, 1990−1995.
(39) Zhang, J.; Dhindsa, N.; Chia, A.; Boulanger, J.; Khodadad, I.; Saini, S.; LaPierre, R. *Appl. Phys. Lett.* **2014**, *105*, 123113.
(40) Dhindsa, N.; Chia, A.; Boulanger, J.; Khodadad, I.; LaPierre, R.; Saini, S. S. *Nanotechnology* **2014**, *25*, 305303.
(41) Du, Q. G.; Kam, C. H.; Demir, H. V.; Yu, H. Y.; Sun, X. W. *Opt. Lett.* **2011**, *36*, 1884−1886.
(42) Bao, H.; Ruan, X. *Opt. Lett.* **2010**, *35*, 3378−3380.
(43) Dayeh, S. A.; Picraux, S. T. *Nano Lett.* **2010**, *10*, 4032−4039.
(44) Glas, F.; Ramdani, M. R.; Patriarche, G.; Harmand, J. C. *Phys. Rev. B: Condens. Matter Mater. Phys.* **2013**, *88*, 195304.
(45) Tan, T. Y.; Li, N.; Gösele, U. *Appl. Phys. A: Mater. Sci. Process.* **2004**, *78*, 519−526.
(46) Zhang, Y.; Aagesen, M.; Holm, J. V.; Jørgensen, H. I.; Wu, J.; Liu, H. *Nano Lett.* **2013**, *13*, 3897−3902.
(47) Marrakchi, G.; Kalboussi, A.; Bremond, G.; Guillot, G.; Alaya, S.; Maaref, H.; Fornari, R. *J. Appl. Phys.* **1992**, *71*, 3325−3329.
(48) Heinke, W.; Queisser, H. J. *Phys. Rev. Lett.* **1974**, *33*, 1082.
(49) Bugajski, M.; Ko, K. H.; Lagowski, J.; Gatos, H. C. *J. Appl. Phys.* **1989**, *65*, 596−599.

DOI: 10.1021/acs.nanolett.5b04554
Nano Lett. 2016, 16, 1237−1243